2-D Simulation for a Spherical Top Inductively Coupled Plasma Source

H-M Wu, M. Li, Y. Yang, C-K Wu

Institute of Mechanics, Academia Sinica, Beijing 100080, China

ABSTRACT: In the present paper, argon plasmas in a bell jar inductively coupled plasma (ICP) source is systematically studied over the range of pressures 5-20 mTorr and power inputs 0.2-0.5 kW. The research work consists of both 2-D fluid model simulation and comparison with global model calculation. The 2-D fluid model simulation with a self-consistent power deposition is developed to describe the Ar plasma behavior as well as predict the plasma parameter distributions. It is found that the uniformity of plasma density in the bell jar top ICP can be significantly improved. Finally, a quantitative comparison between the global model and the fluid model is made to estimate their validity.

I. INTRODUCTION

The limitation of radio frequency (rf) diodes have led to the development of new plasma sources, such as the electron cyclotron resonance (ECR) plasma source and inductively coupled plasma (ICP) sources that operate at low pressure and high plasma density. Plasma densities in these enhanced plasma sources can reach $10^{11}\sim10^{12}/cm^3$ with neutral pressures in the range of $1\sim20$ mTorr.[1-2] As a new kind of plasma source, ICP has appealed to many scientists due to its structural simplicity.[3] Accompanying this surge of new generation of plasma source study there has been an effort to understand the plasma parameters in ICP.[4-8]

Low pressure ICP has been employed for etch processing starting a few years ago.[9] Since then a lot of research work has been carried out all over the world.[2,4] In order to develop this etching tool and provide some predictions for design, we have been carrying out several studies of ICP.[3-8] Our latest ICP employs a new design in which a bell jar quartz top is used to reduce the thickness of dielectric layer for less cost of the quartz. More uniform plasmas can be obtained by adjusting both the wafer stage position and the inductive coil geometry.

II. THEORETICAL MODELING

Geometry descriptions: The geometry of the bell jar top ICP chamber is shown in Fig.1. The bottom chamber is made of stainless steel with radius r=12 cm and height L=8 cm, respectively. The top bell jar cover, with radius of curvature 13 cm, is isolated whereas the bottom chamber is grounded. The dome cover is made of quartz with 0.5 cm thickness.[8]

A. GLOBAL MODEL

A global model, established by M. A. Lieberman and R. A. Gottscho, has been proved quite reliable and simple for estimating the plasma parameters in an enhanced plasma source.[1,4] The global model calculation for the dome top ICP was previously done. For convenience to the readers, we give a brief summary here.

The expression of the rate coefficients for the inelastic process all have the same form

$$K_i(T_e)=\sigma_i v_e \exp(-E_i/kT_e) \qquad (1)$$

where σ_i and $v_e=(8kT_e/\pi m_e)^{1/2}$ are scattering cross section and mean electron thermal speed, respectively. The subscript "i" denotes the *ith* inelastic scattering.

Global particle balance requires:

$$K_{iz}NnV = \Gamma \equiv \Gamma_b+\Gamma_s+\Gamma_t \qquad (2)$$

where K_{iz}, N, n, V, Γ_b, Γ_s, and Γ_t are the ionization rate, the neutral gas density, the plasma density, chamber volume, the ion fluxes on the bottom wall, side wall and top dome wall, respectively. These fluxes can be expressed as

$$\Gamma_b = \pi r^2 h_L\, n\, u_B, \qquad \Gamma_s = 2\pi r L h_R n\, u_B.$$

$$\begin{aligned}\Gamma_t &= \int_S n u_B (h_L \cos\theta + h_R \sin\theta) dS \\ &= 2\pi R^2 n\, u_B \int_S (0.5 h_L \sin 2\theta + h_R \sin^2\theta) d\theta \\ &= \pi R^2 n\, u_B (a h_L + 2 b h_R),\end{aligned}$$

where $a = \int_s \sin 2\theta d\theta = 0.85$, $b = \int_s \sin^2\theta d\theta = 0.41$, and the integration domain s is the top spherical surface, respectively.

$$h_L = 0.86(3+0.5L/\lambda_i)^{-1/2}, \quad h_R = 0.8(4+ r/\lambda_i)^{-1/2},$$

where $\lambda_i = 1/\sigma_i N$ is the ion-neutral mean free path.

Electron temperature T_e can be obtained by solving the following equation,

$$K_{iz}(T_e)/u_B = \Gamma/u_B NnV \equiv 1/Nd_{eff} \qquad (3)$$

where $d_{eff}=V/\pi[\, h_L(r^2 + R^2 a) + 2h_R(rL + R^2 b)]$.

Plasma density n and ion current density on wafer J_b can be derived in the following procedure: Define the collisional energy lost per electron-ion pair created

$$\varepsilon_c=\varepsilon_{ion} + [K_{ex}\varepsilon_{ex}+K_{me}\varepsilon_{me}+K_{el}\varepsilon_{el}]/K_{ion} \qquad (4)$$

where ε_{ion} =15.75eV, ε_{ex}=14.1eV, ε_{me}=12eV and $\varepsilon_{el}=3mkT_e/M$ are the energy lost per electron, for Ar, as a result of ionization, electronic excitation, metastable creation and elastic collisions, respectively. The total energy lost per electron-ion pair in the system can be expressed as follows,

$$\varepsilon_L=\varepsilon_c + 5.2\ kT_e + 2kT_e = \varepsilon_c + 7.2\ kT_e \qquad (5)$$

The overall global energy balance for the ICP can be written in terms of ε_L as

$$P_{abs}=u_B n_S A_{eff} \varepsilon_L \qquad (6)$$

where $n_S A_{eff} = \pi r^2 h_L + 2r\pi n L h_R + \int_s n(h_L cos\theta + h_R sin\theta)d\theta$, P_{abs} is power absorbed in the plasma and n_S the plasma density at the pre-sheath, respectively. Then there is the equation

$$n=P_{abs}/\{eu_B\varepsilon_L [\pi r^2 h_L + 2r\pi L h_R + \int_s (h_L cos\theta + h_R sin\theta)d\theta]\} \qquad (7)$$

can be solved directly for plasma density.

B. 2-D FLUID MODEL

1. Fluid equations

The basic assumptions of the model are: (1) The neutral gas flow is omitted. (2) The ion temperature is the same as that of the neutral gas. (3) The inductive coils are simplified as three coaxial circular coils. (4) The electron distribution is roughly considered as Maxwellian. (5) Neutral density and temperature are assumed to be uniform in the chamber.

Three neutral argon gas pressures 5 mTorr, 10 mTorr and 20 mTorr are considered separately in the simulation. The total power inputs are 200W and 500W, respectively.

The time average equations for electrons and ions are

$$\nabla \cdot J_e = R_i \qquad (8)$$

$$\nabla \cdot J_i = R_i \qquad (9)$$

$$\nabla \cdot Q_e = q_j - \Sigma R_k \varepsilon_k e \qquad (10)$$

where

$$J_e = -\mu_e n_e E_s - (k/m_e \nu_{eN})\nabla(n_e T_e)$$

$$J_i = -\mu_i n_i E_s - (2k/m_i \nu_{iN})\nabla(n_i T_i)$$

$$Q_e = 2.5(kT_e J_e) - 2.5(k^2/m_e \nu_{eN}) n_e T_e \nabla T_e$$

$$\mu_e = e/m_e \nu_{eN}, \qquad \mu_i = 2e/m_i \nu_{iN}$$

$$q_j = 1/T \int_T \sigma E^2\, dt$$

The total input power can be written as

$$P_t = 2\pi \iint q_j\, rdrdz$$

The collision rate R_k can be expressed as $R_k=K_k n_e N$, where the subscript k= iz, ex, me and el have the same definitions as Eq.(4). The above set of fluid

equations is closed with Poisson's equation with regard to the space charge to the electrostatic potential,

$$\varepsilon_0 \nabla^2 \phi = e(n_e - n_i)$$

where ε_0 is the permittivity of free space.

The boundary conditions are the same as our previous work[7], i.e. $n_e = \phi = \mathbf{n}\cdot\nabla n_i = \mathbf{n}\cdot\nabla T_e = 0$ on the metallic wall; on the axis there are $\partial n_e/\partial r = \partial n_i/\partial r = \partial\phi/\partial r = \partial T_e/\partial r = 0$. Based on the thin plasma sheath model, we have the analytical results to obtain the boundary conditions on the quartz wall as following

$$J_{ew} = (1/4)\, n_{es} v_{es} \exp(-e\Delta\phi/kT_e)$$

$$J_{iw} = n_{is} u_B$$

$$\phi_w = \phi_s + (kT_{es}/e)\, ln(4J_{iw}/n_{es}v_{es})$$

where J_{ew} and J_{iw} are their normal components to the wall, the subscript s represents the plasma-sheath boundary position, boundary plasma potential $\Delta\phi = \phi_w - \phi_s$ and the electron energy flux on the top $Q_{ew} = J_{ew}(2kT_{es} + e\Delta\phi)$, respectively.

2. Electromagnetic equations

The electric field consists of the inductively coupled field and the plasma static field. The net field is $\mathbf{E} = \mathbf{E}_I + \mathbf{E}_p$. The plasma static field is determined by Poisson equation:

$$\nabla^2\phi = -\nabla\cdot\mathbf{E} = -e/\varepsilon_0(n_i - n_e) \qquad (11)$$

Because of the axial symmetric assumption, the inductive electric field which has only azimuthal component is written as

$$E = E_1 \cos\omega t + E_2 \sin\omega t$$

The equations for E are:

$$\nabla^2 E_1 - E_1/r^2 - \xi\sigma\omega E_2 = 0 \qquad (12)$$

$$\nabla^2 E_2 - E_2/r^2 + \xi\sigma\omega E_1 = 0 \qquad (13)$$

where $\xi = 4\pi\times10^{-7}$ H/m, $\sigma = (n_e e^2/m_e\nu_{eN})[1+(\omega/\nu_{eN})^2]$ is plasma electric conductivity, ν_{eN} is the electron-neutral collision frequency. The boundary condition for eqs.(12-13) are $E = 0$ on the metallic wall and the axis. The boundary condition on the quartz bell jar is determined by the coil current $I = I_0\cos\omega t$ and the inductive plasma current $\sigma_{ij}E_{1,2}\Delta z_i\Delta r_j$ at the nearest cell to wall. The detailed deduction and computational method can be found from ref[7].

C. RESULTS AND DISCUSSION

Fig.2 is the electron temperature distribution with 10 mTorr neutral pressure and 200W power input. As in our previous result, T_e is quite uniform in the bulk plasma. The difference between the maximum on the upper centerline and minimum at the bottom is only 0.3 eV. With this relatively flat temperature profile, we can expect the spatial profiles for ionization rate and plasma density to be quite similar. The plasma potential is shown in Fig.3. It can be seen that the maximum at the center is about 14V and the minimum at the corner is 11V. It implies that the plasma static electric field E_p is small. Fig. 4 is the plasma

density profile and contours with the same operational conditions. The plasma density near the bottom is extremely uniform. This is one of the advantages for the bell jar top ICP. It is found that the maximum exceeds $10^{11}/cm^3$. Fig. 5 is the comparison for electron temperatures between the global model and the simulation. Plasma densities comparison between global model and simulation is shown in Fig.6. It seems that the simulation agrees reasonably well with the global model. The difference might come from the neutral gas uniformity assumption. The global model can give a quick estimation whereas the fluid can provide a spatial profile for the parameters.

It is well known that the uniformity in conventional ICP is primarily determined by the inductive coil geometry. However, in the bell jar top ICP, there are two ways to improve the uniformity. One is to adjust the inductive coil configuration and the other is to change the stage position. Therefore the uniformity in the bell jar top ICP can be significantly improved. In addition to the uniformity, it is obvious that the bell jar quartz top can be easily made because it is thin. Experimental measurement for plasma parameters, by means of a turned Langmuir probe, is in progress and will be published soon.

D. ACKNOWLEDGEMENT

The authors acknowledge the support from the Presidential Foundation of Chinese Academy of Sciences.

References

[1] M.A.Lieberman and R.A.Gottscho,"Design of High Density Plasma Sources for Material processing" in *Physics of Thin Films* edited by M.Francombe and J.Vossen, Academic Press, (1994).

[2] D.B.Graves, "Plasma Processing," *IEEE trans plasma science*, 22,(1994)31.

[3] H-M Wu, D.W.Dong and J.Y.Xu, *Material of Electronics*,12(1994)7, (in Chinese).

[4] R.Stewart, P. Vitello and D.B.Graves, *J.Vac. Sci. Technol.*, **B12**,(1994)478.

[5] J. H. Keller, J. C. Forster, and M. S. Barnes, *J. Vac. Sci. technol.* **A11**, (1993)2487.

[6] J.Hopwood,Appl.Phys.Lett. 62,(1993)940.

[7] M.Li, H-M Wu,Y-M Chen, *IEEE trans. Plasma Sci.* (1995) to be published.

[8] H-M Wu, M. Li and Y-M Chen, Chinese Phys. Lett., 12, 5(1995)281

[9] LAM Research Corperation, U. S. Patent No.4948458(14,August,1990)

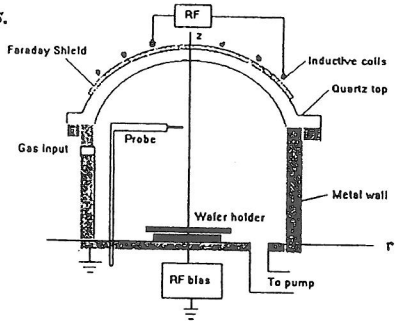

Fig. 1 The geometry of the ICP chamber.

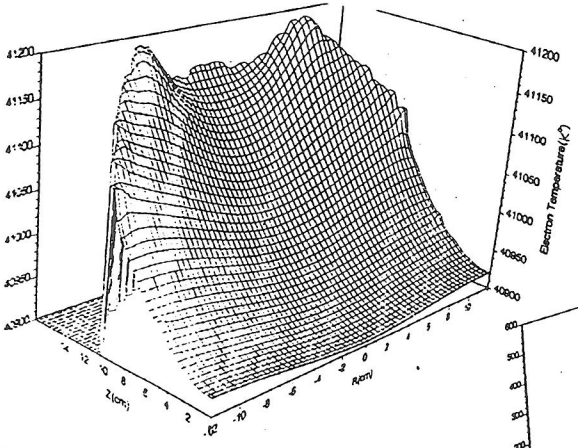

Fig. 2 Spatial profile of electron temperature.

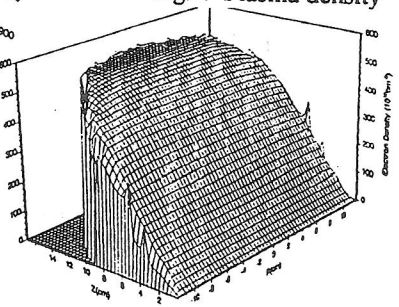

Fig. 4 Plasma density

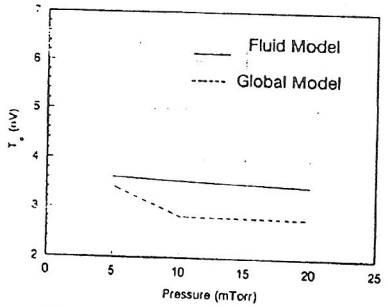

Fig. 5 T_e comparison of global model and simulation.

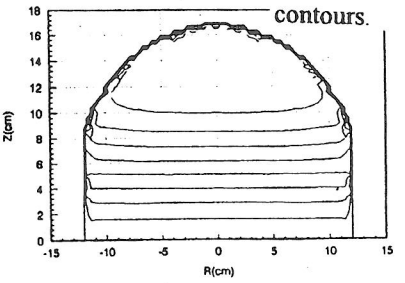

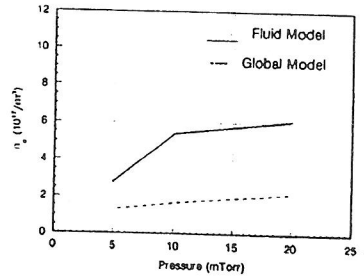

Fig. 6 Density comparison of global model and simulation.

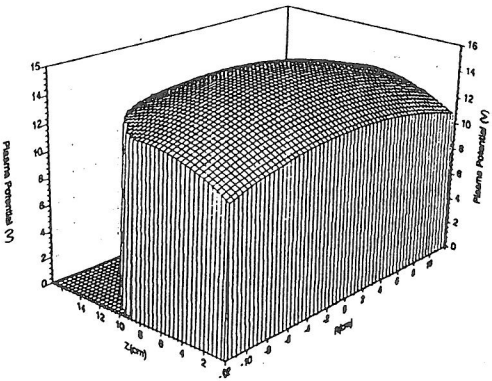

Fig. 3 Spatial profile of plasma potential.